PROCEEDINGS OF THE ROYAL SOCIETY A

Proc. R. Soc. A (2007) **463**, 1393–1408
doi:10.1098/rspa.2007.1829
Published online 6 March 2007

On a ferroelastic mechanism governing the toughness of metastable tetragonal-prime (t') yttria-stabilized zirconia

By C. Mercer, J. R. Williams, D. R. Clarke and A. G. Evans*

Materials Department, College of Engineering, University of California Santa Barbara, Santa Barbara, CA 93106-5050, USA

This article investigates the toughness of yttria-stabilized zirconia (YSZ) with the tetragonal-prime (t') structure. Such materials are used as durable thermal barriers in gas turbines. Their durability has been attributed to high toughness, relative to materials in the cubic phase field. Based on prior literature, a ferroelastic toughening mechanism is hypothesized and this assertion is examined by characterizing the material in the wake of an indentation-induced crack. Assessment by transmission electron microscopy, Raman spectroscopy and optical interferometry has affirmed the existence of a process zone, approximately 3 μm in width, containing a high density of nano-scale domains, with equal proportions of all three crystallographic variants. Outside the zone, individual grains contain a single variant (no domains) implying that the toughening mechanism is controlled by domain *nucleation* (rather than the *motion* of pre-existing twin boundaries). The viability of the ferroelastic toughening mechanism is assessed using a process zone model that relates the observed toughening to the stress/strain hysteresis accompanying domain formation. Based on the measured process zone size, the known tetragonality of t'-7 wt% YSZ and the enhancement in toughness relative to cubic YSZ, consistency between the model and the observed toughening is demonstrated for a reasonable choice of the coercive stress.

Keywords: ferroelastcity; toughening; yttria-stabilized zirconia; transmission electron microscopy

1. Introduction

The application of 7 wt% yttria-stabilized zirconia (YSZ) as a thermal barrier coating (TBC) on airfoils used in aero and power generation gas turbines has motivated interest in its thermomechanical properties. In the earliest implementations, the designs placed minimal reliance on the thermostructural integrity of the YSZ, so its mechanical properties were of secondary relevance. As the technology has advanced, knowledge of specific high temperature properties has become increasingly important. Among these, the fracture toughness is especially critical, owing to its central influence on the mechanisms that limit the durability. The mechanisms affected by the toughness include (i) large-scale

* Author for correspondence (agevans@engineering.ucsb.edu).

Received 15 December 2006
Accepted 5 February 2007

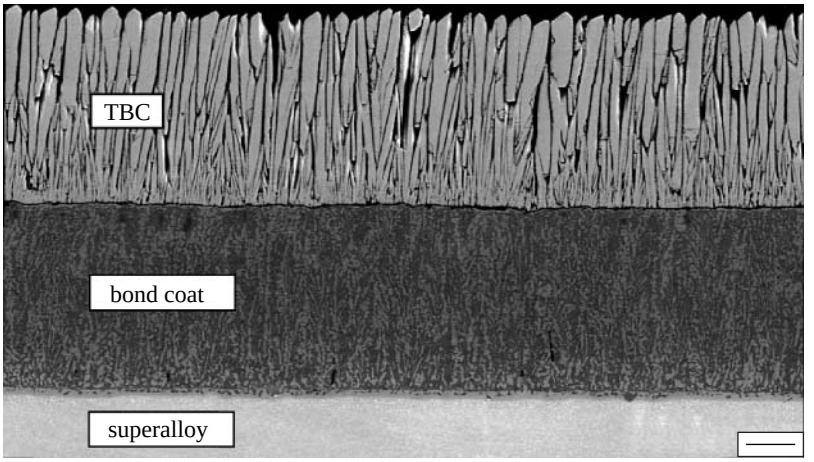

Figure 1. Image of a columnar thermal barrier oxide produced by electron beam physical vapour decomposition (EB-PVD). The columnar structure and the gaps between the columns preclude toughness measurements without densification. Scale bar, 50 μm.

delamination caused by strain misfit with the substrate, especially under thermal cycling conditions (Tolpygo & Clarke 1999; Evans *et al.* 2001; Mumm *et al.* 2001; Clarke & Levi 2003), (ii) material loss due to erosion and foreign object damage (FOD) (Chen *et al.* 2003), and (iii) delamination caused by penetration of molten calcium magnesium aluminosilicate (CMAS; Borom *et al.* 1996; Mercer *et al.* 2005). Given the importance of toughness, measurements are sparse for materials having the compositions, phases and microstructures found in actual thermal barrier systems. The purpose of the present assessment is to provide a perspective on mechanisms that dictate the toughness of YSZ and related compositions. The emphasis is on the materials generated at relatively low temperature (approx. 1000°C) from the vapour phase, particularly by electron beam physical vapour deposition (EB-PVD). Such materials contain phases that differ from those in materials with the same composition generated by sintering at higher temperature (Lange 1982). The 7 wt% YSZ used in most gas turbine applications is a metastable, single-phase tetragonal-prime, t', having a columnar microstructure (figure 1), and $\langle 100 \rangle$ growth texture (Schulz *et al.* 2003). At this composition, the t'-phase has tetragonality (ratio of c-axis to a-axis lattice dimensions), $c/a-1=1.1\%$.

The focus of this investigation is on the mode I toughness, directly pertinent to failure by erosion, FOD and CMAS degradation (Chen *et al.* 2003; Mercer *et al.* 2005). Other failure mechanisms are controlled by the mode II toughness, such as edge and buckle delaminations (Choi *et al.* 1999). Since the mode II toughness is always larger than that in mode I (sometimes by over an order of magnitude; Suo & Hutchinson 1989), this investigation provides an understanding of the baseline fracture energy appropriate to TBC systems.

The article is organized as follows: (i) a synopsis of the known mechanisms of toughening in YSZ is presented, emphasizing the phases and the compositions applicable to each, (ii) a method for estimating the toughness of t'-materials made from the vapour phase is presented, (iii) procedures capable of characterizing process zones adjacent to cracks are used to measure features

affecting the toughness, and (iv) process zone toughening models are used to interpret the measurements and to provide a direction for future investigation of materials with higher toughness.

2. Synopsis of the toughness of yttria-stabilized zirconia

YSZ materials can exist in a variety of crystallographic phases depending on the yttria concentration and on the process used to make them. Available measurements of the ambient mode I toughness of a number of yttria-stabilized materials over the relevant compositional range are summarized in figure 2*a*,*b* (Lange 1982; Evans & Cannon 1986; Becher & Swain 1992). Also shown for comparison are the toughness levels (generally steady-state) for other ceramics and glasses (Wachtman 1996). Strikingly, the toughness of YSZ materials encompasses the entire range. Partially stabilized materials (denoted as tetragonal zirconia polycrystals; TZP), prepared by high temperature processes (such as sintering) have the highest toughness: a typical toughness is, $\Gamma_{ss} \approx 210$ J m^{-2} for 4 wt% YSZ (Green *et al.* 1989). Conversely, the cubic materials are among the most brittle: $\Gamma_{ss} \approx 6$ J m^{-2} for 20 wt% YSZ (Marrow *et al.* 1994). Moreover, for the compositions commonly used in TBCs, a wide toughness range exists, even at fixed composition: $45 \leq \Gamma_{ss} \leq 150$ J m^{-2} for 7 wt% YSZ. The highest values emerge from processing routes that create materials in the two-phase (cubic/tetragonal) equilibrium phase field. These materials exhibit transformation toughening, enabled by the tetragonal-to-monoclinic ($t \rightarrow m$) phase transformation during crack extension (Evans & Cannon 1986). Lower values apply to materials processed using vapour phase routes that result in the metastable t'-phase (Evans 1990). Nevertheless, the latter are preferred in gas turbine applications, because coatings in this phase field exhibit the greatest thermal cyclic durability (Levi 2004). The assertion is that the associated toughness, while not exceptional, is retained at elevated temperatures (for reasons elaborated below), whereas transformation toughening is only operational at low-to-moderate temperatures (Evans & Cannon 1986). The present study focuses on the toughness of YSZ with t'-phase, relative to that in the cubic field.

When the martensitic $t \rightarrow m$ transformation is suppressed, the toughening exhibited by tetragonal materials (relative to their cubic counterparts) has been attributed to ferroelastic domain switching (Virkar & Matsumoto 1986; Srinivasan *et al.* 1989; Chan *et al.* 1991). Most unstrained ferroelastic materials contain equal proportions of domains with three orthogonal variants separated by 90° {110} twin boundaries. Upon unidirectional loading, say along ⟨100⟩, one set of variants can switch orientation. When this happens, there is an associated strain, $\varepsilon^T = (1/3)(c/a - 1)$ (figure 3) which occurs at a 'constant' coercive stress, σ^T. (In accordance with the volume constancy of the ferroelastic mechanism, it is assumed that this coercive stress is identical under tensile and compressive conditions.) Generally, the switching is irreversible, resulting in permanent strain. Whenever cracks extending in such materials cause one of the variants to switch (Jue & Virkar 1990), toughening can occur owing to the associated stress/strain hysteresis (figure 3). Stress/strain measurements on YSZ in the compositional range 6–16 mol% yttria have indicated that the coercive stress (and the hysteresis) are relatively temperature invariant (σ^T varies from

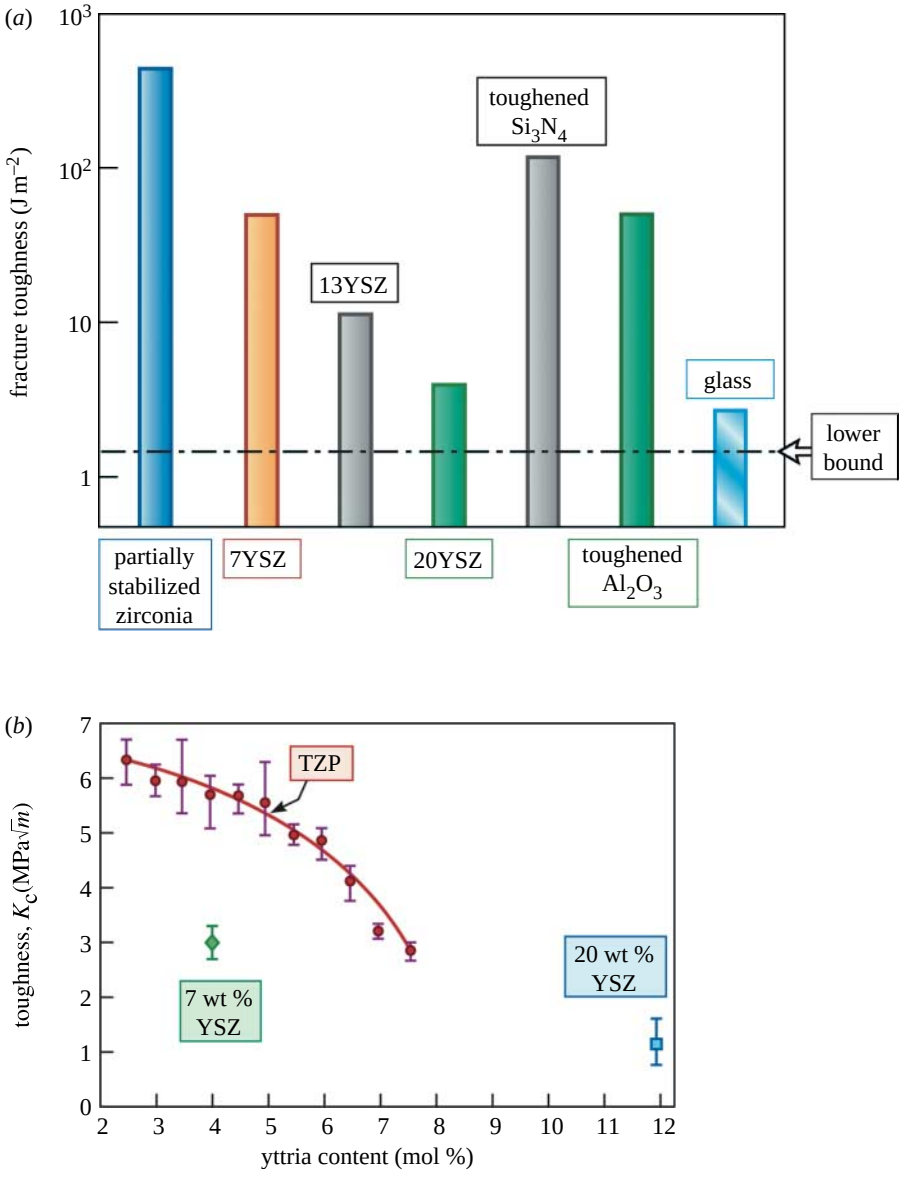

Figure 2. (*a*) Histogram of toughness levels found in a range of YSZ materials and comparisons with other ceramics. Note that the toughness scale is logarithmic. (*b*) The effects of composition on the toughness of a range of YSZ materials. The TZP materials are two-phase (cubic/tetragonal), made by sintering. The 7 wt% YSZ material is t', made by vapour deposition. The 20 wt% YSZ is in the cubic phase field.

700 to 500 MPa between 500 and 1400°C; Baither *et al.* 2001). The implication is that the toughness associated with ferroelastic switching will also be insensitive to temperature.

These prior assessments have relied upon *pre-existent domains* capable of switching in the crack stress field. Yet, the available microscopy evidence precludes the existence of domains in either vapour-deposited or plasma-sprayed coatings of

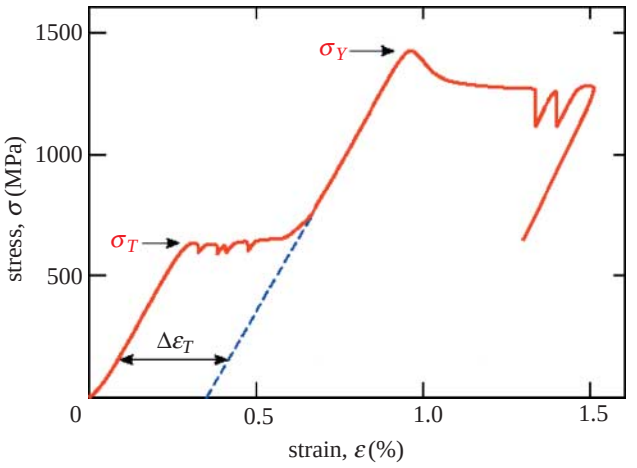

Figure 3. A compressive stress/strain response at 500°C for a 3 mol% YSZ single crystal. Note the inelastic strain induced at the coercive stress. Reproduced from Baither *et al.* (2001).

t'-7 wt% YSZ. Rather, in vapour-deposited systems, each column is a single crystal (incorporating sub-grains). Consequently, should a ferroelastic mechanism be identified, it will differ qualitatively from that discussed in the prior literature.

3. Toughness measurements

Measurement of the short crack, mode I toughness of vapour-deposited YSZ materials has proven challenging. The methods developed for large, dense ceramics cannot be used with a columnar TBC owing to the fragility of the inter-columnar regions. Indentation methods can be applied (Lawn 1975; Evans & Charles 1976; Anstis *et al.* 1981; Cook & Pharr 1990) provided that the material is first 'densified' at temperatures and pressures that retain the t'-phase. For the present work, a dense material has been prepared from the amorphous powders deposited on the cold walls of a commercial EB-PVD system and consolidated by hot-pressing. The steps taken to ensure that the hot pressed material did not decompose into an equilibrium mixture of cubic and tetragonal phase during densification are described elsewhere (Nychka *et al.* 2006). Briefly, the powders were hot consolidated at 1500°C, below the T_0 line for the tetragonal-to-cubic transformation, thereby assuring that the t'-phase was retained. Analysis by both Raman spectroscopy and X-ray diffraction confirm that the resulting material retains its metastable tetragonal-prime structure. The grain size of the resulting dense material is in the range of 0.5–1 μm. Impressions emplaced into this material by a Vickers indenter generate well-delineated radial cracks (figure 4). To obtain explicit measurements, the indentation fracture toughness formula relating toughness to the crack length (ℓ) and indentation load is used (Lawn 1975; Anstis *et al.* 1981)

$$\Gamma = \xi P^2/H\ell^3, \tag{3.1}$$

where P is the indentation load, H is the hardness of the (dense) material (measured *in situ*) and the non-dimensional coefficient, $\xi = (0.016)^2$. The results indicate that, for t'-7 wt% YSZ, the toughness is $\Gamma_{ss} = 45 \pm 5\ \mathrm{J\,m^{-2}}$, while that for the cubic 20 wt% YSZ is, $\Gamma_{ss} = 6 \pm 2\ \mathrm{J\,m^{-2}}$ (Marrow *et al.* 1994; Watanabe *et al.* 2004).

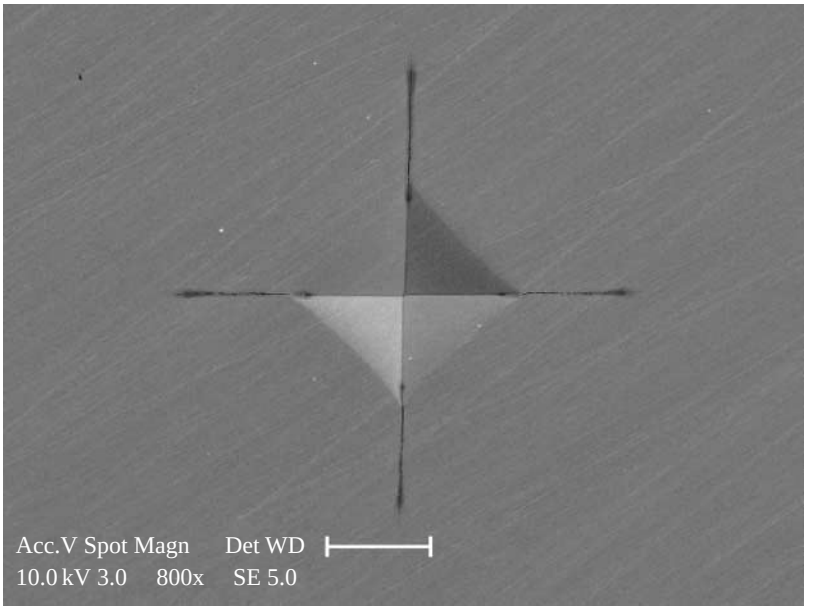

Figure 4. Indentation cracks in a dense body of 7 wt% YSZ (courtesy of F. Pitek). Scale bar, 20 μm.

4. Characterization of the process zone

Establishing a toughening mechanism requires that hysteretic phenomena be identified within a process zone in the 'wake' of an induced crack (figure 5*a*). The governing hysteresis is predicated on a local stress/strain response of the type indicated on figure 5*b*, typical of the strains occurring at the coercive stress in association with ferroelastic domain switching (Baither *et al.* 2001). Two complementary approaches are used.

Method I. Recall that a process zone embodies permanent strains, symmetrically on both sides of the crack (Evans 1990), and that, at the intersection of the crack with a free surface, these strains cause the surface to distort from an initially flat plane. Accordingly, a method capable of detecting the uplift and ascertaining its spatial extent provides a means for mapping the entire process zone. Optical profilometry has the requisite attribute: namely, it can detect very small height differences over a wide spatial extent. Since surface uplift can be attributed to either a ferroelastic or a $t \rightarrow m$ transformation mechanism, it is essential to check on the phases present within the zone by collecting Raman spectra from regions around the crack.

Method II. Complementary and confirmatory information is provided by transmission electron microscopy (TEM). The rationale being that ferroelastic domains can be distinguished from electron diffraction patterns and highlighted using dark-field contrast (Chan *et al.* 1991). Using the focused ion beam (FIB) system to obtain thin foils immediately adjacent to the crack plane and comparing with foils obtained from a remote location, the occurrence of crack-induced ferroelasticity can be ascertained.

(*a*) *Optical interferometry*

The surfaces of the indented t'-7 wt% YSZ samples were characterized using an optical imaging Mirau interferometer (Wyko NT1100 optical profiling system) to quantify the surface relief as a function of position around the cracks. A highly localized surface uplift was apparent on both sides of the cracks that extended continuously to the crack-tips (figure 6*a*). Height profiles (figure 6*b*) allowed the uplift zone to be quantified. Defining the process zone from the contour at which the surface relief was half of the maximum height, the width was found to be $h \approx 3\,\mu\text{m}$. Within the limits of the lateral spatial resolution, the width of the uplift zone was found to be invariant along the length of the crack. Although the interferometer had insufficient lateral spatial resolution to reveal either the individual domains or fine details of the zone shape, the zone width was found to be commensurate with the zone size measured by TEM, described below. Together these measurements provide unambiguous evidence that a crack wake process zone is created in t'-7 wt% YSZ upon crack extension. It is noted that the image in figure 6*a* has been oriented to emphasize the uplift around crack A. This diminishes the contrast of crack C. Also, if the crack is not precisely normal to the surface, the relief is asymmetrical and can become masked by any mode III displacements perpendicular to the surface such as crack B.

(*b*) *Raman spectroscopy*

To exclude the possibility of crack-induced transformation to the monoclinic phase (as occurs in transformation toughening), Raman spectra were recorded using an optical probe that focuses down to approximately 1 μm diameter. At all locations, including crack tips and the corner of the indentations, the material remained t'. A typical Raman spectrum recorded at one of the indentation cracks using an approximately 2 μm probe is presented on figure 7. Had any monoclinic phase been present, a peak would have occurred at the frequency arrowed on the figure. Previous work, using less sensitive instrumentation, has shown that transformation zones as small as 5 μm can be readily detected by the presence of monoclinic peaks in the Raman spectra (Clarke & Adar 1982).

(*c*) *Transmission electron microscopy*

Specimens for TEM analysis, prepared using an FEI Strata 235 FIB instrument, were taken from two locations relative to the indentation impression (figure 8). One encompassed the crack along a normal, close to its tip, assuring that the section resides well outside the plastic zone of the indentation. The second location was within material away from the indentation. Bright-field images close to the crack plane reveal a pattern of nanoscale domains (figure 9*a*). While it has not been possible to obtain images with better contrast, owing to the small scale of the individual domains, the appreciable strain contrast variations and the ion damage, the presence of twin variants is apparent in two orthogonal orientations (shown in more detail by the higher magnification inset in figure 9*a*). Tilting to capture a variety of diffraction conditions establishes that most of the grains adjacent to the crack

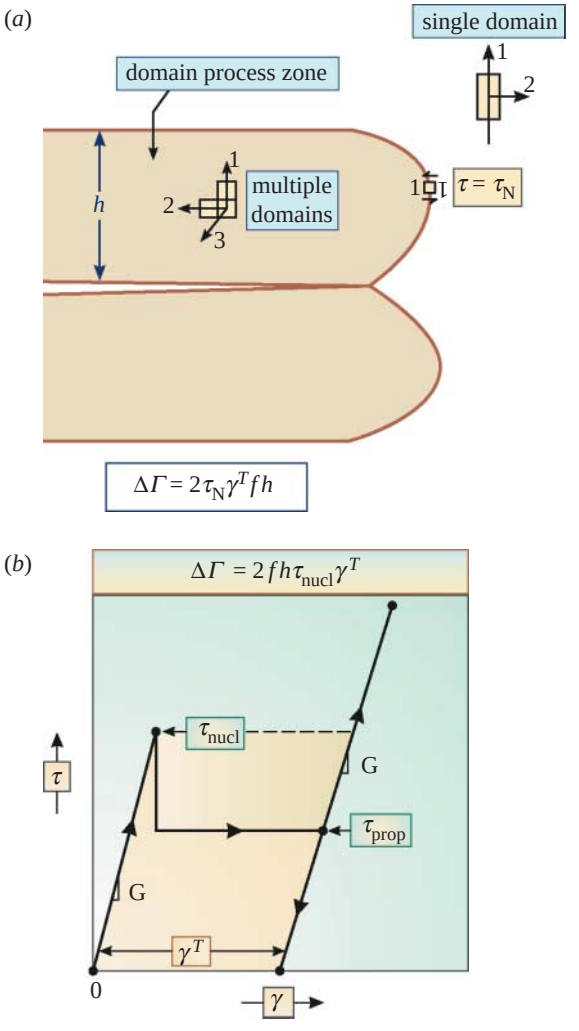

Figure 5. (*a*) A schematic of a ferroelastic process zone. (*b*) A proposed stress/strain curve representing the ferroelasticity in the present situation, where nucleation is important. The mechanism is activated when the shear stresses around the crack reach τ^T, resulting in a permanent shear strain, γ^T.

contain such domains. In the remote section, similar tilting did not reveal contrast that could be attributed to domains (figure 9*b*). Furthermore, upon traversing both sides of the crack, the width of the zone containing domains has been ascertained to be, $h \approx 3\,\mu\text{m}$ (figure 10), entirely consistent with the foregoing uplift measurements made using interferometry. While there is not a well-delineated boundary demarking the edge of this zone, there is clearly a higher fraction of grains containing domains within approximately 3 μm of the crack (figure 10).

To determine the crystallographic nature of the domains in the process zone, selected area electron diffraction was performed. This involved tilting to a ⟨111⟩ zone axis and seeking the presence of {112} superlattice reflections. The

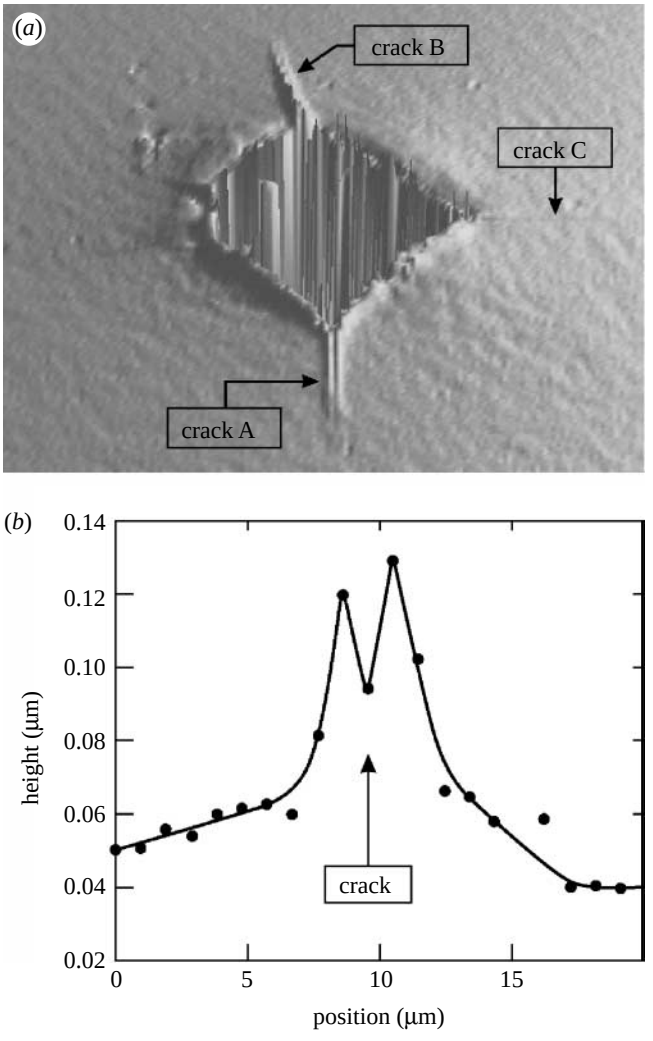

Figure 6. (*a*) Interferometric image illustrating the localized surface uplift on both sides of a crack, A, emanating from an indentation impression. (*b*) Height variation across crack A. The data points correspond to individual pixels and their spacing is at the minimum lateral spatial resolution of the interferometer, approximately 1 μm. From this measurement, the width of the process zone is approximately 3 μm.

number of such reflections in the diffraction pattern corresponds directly to the number of twin variants, as indicated by the schematics in figure 11 (Chan *et al.* 1991). A ⟨111⟩ diffraction pattern obtained from a grain with a large number of domains (figure 11*a*) reveals the presence of all three nonparallel {112} super-lattice reflections (highlighted by the white arrows on the figure). Comparison with the schematic indicates that all three variants are present. In marked contrast, the corresponding {112} reflection from a region outside the process zone (figure 11*b*), affirms that only a single (parent) variant exists in each grain.

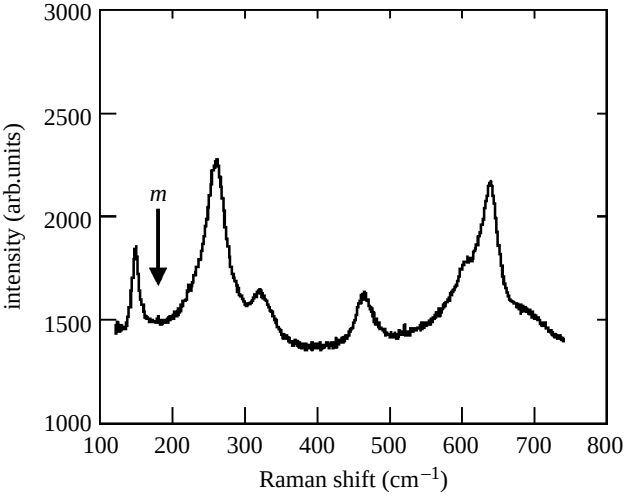

Figure 7. Raman spectrum obtained from a crack tip indicating that the structure remains tetragonal (t'). Any transformation to monoclinic would be evident from the appearance of a peak at the frequency indicated by the arrow.

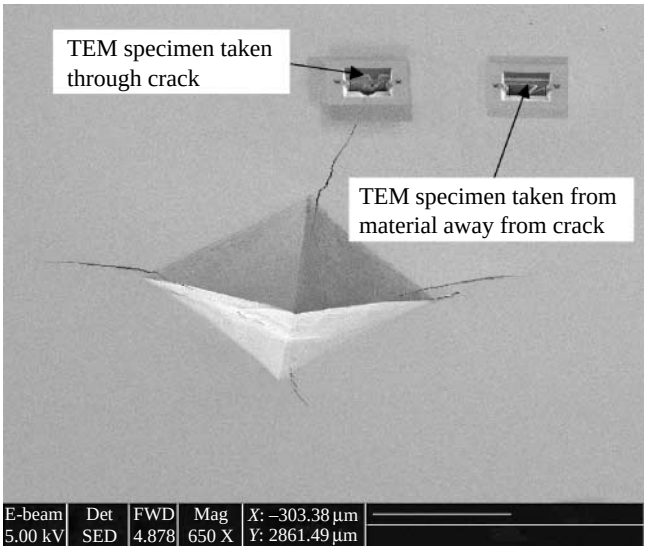

Figure 8. Scanning electron micrograph of micro-hardness indentation and associated cracking, showing the locations from where TEM specimens were taken by FIB. The image has been tilted to provide a perspective that includes the cracks and the sites where the FIB sections were extracted. Scale bar, 50 µm.

Dark-field images formed using the {112} reflections indicated roughly equal proportions of the three variants inside the process zone (figure 12). Again, the small width and the associated strain fields compromise the resolution and quality of the images. Numerical fast Fourier transforms of the individual images also showed distinctive streaking indicative of domain alignment in each variant. None was evident in the grains well away from the crack.

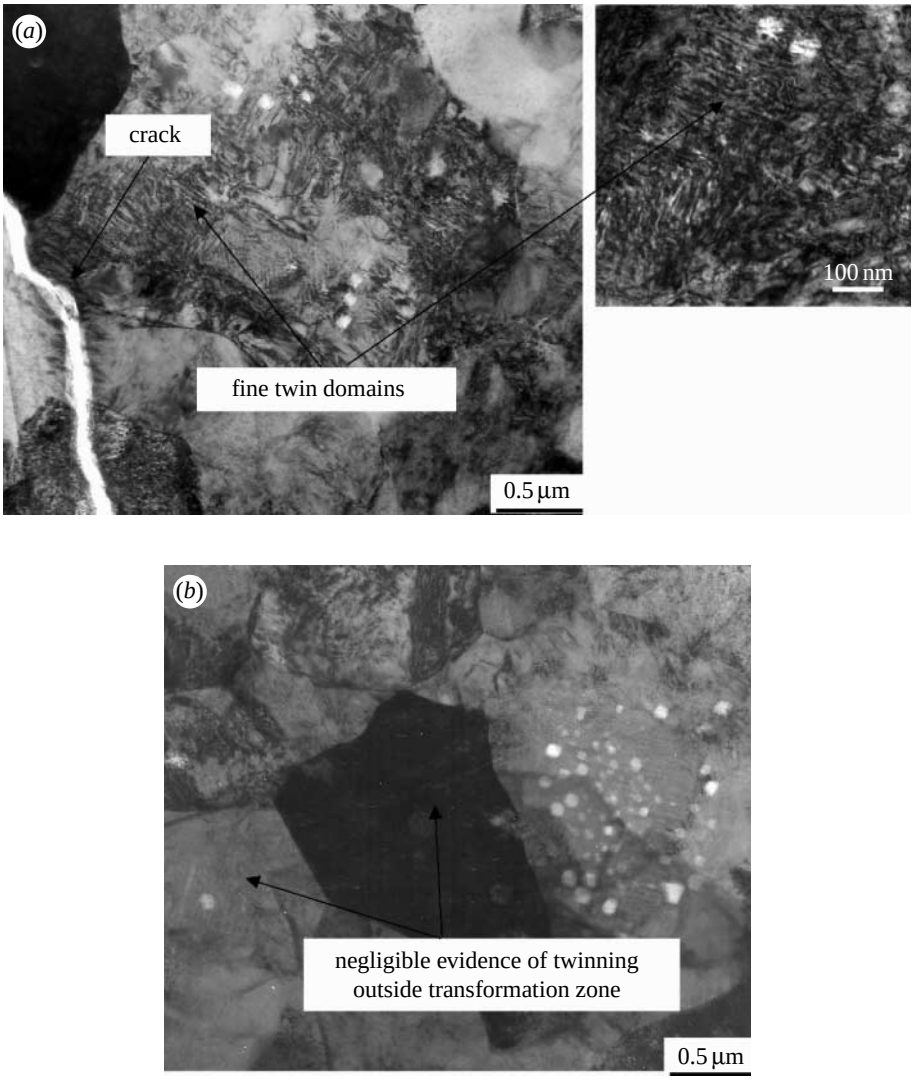

Figure 9. Bright-field TEM images. (*a*) Ferroelastic domains inside a grain within the process zone (inset shows domains in greater detail) and (*b*) an unaffected grain outside the process zone.

5. Discussion and implications

The preceding observations present compelling evidence for the irreversible formation of ferroelastic domains in a process zone on either side of a crack formed by indentation. According to models for the toughening due to the non-reversible ferroelasticity, the energy dissipated per unit volume of transformed material is associated with the resultant area under the stress/strain $[\tau^T(\gamma^T)]$ curve depicted on figure 5*b*. Under steady-state conditions, the increase in toughness (energy per area) has magnitude (Evans 1990)

$$\Delta\Gamma_{ss} = 2f\tau^T\gamma^T h, \tag{5.1}$$

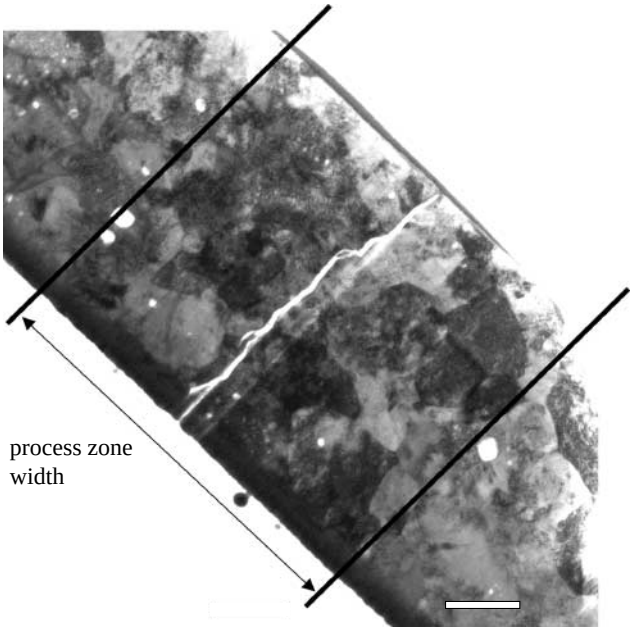

Figure 10. Bright-field TEM image showing the width of the process zone around an indentation crack. A greater volume fraction of grains containing domains is apparent within the process zone. Scale bar, 1 μm.

where h is the width of the process zone (figure 5*a*) and f is the volume fraction of the material within the zone that experiences the strain γ^T. Equation (5.1) can be used to determine whether the measured toughness of t'-7 wt% YSZ derives from ferroelasticity. It is conducted in the following manner. In equation (5.1) the four quantities $\Delta\Gamma_{ss}$, f, γ^T and h can all be ascertained from the foregoing information. The only unknown is the coercive stress, τ^T. Consequently, if equation (5.1) is used to infer the operative τ^T, comparison with figure 3 (Baither *et al.* 2001) can be used to assess consistency.

Outside the process zone, each grain consists of a single variant. Inside the zone, domains are found with all three orthogonal variants. The associated coercive strain is thus directly related to the tetragonality by $\gamma^T=(2/3)(c/a-1)$. The TEM observations indicate that the fraction of material transformed into domains within the process zone, $f\approx 0.8$. The increase in toughness caused by the mechanism is taken as the difference between that for t'-7 wt% YSZ (toughened) and cubic-20 wt% YSZ (not toughened). The difference is $\Delta\Gamma_{ss}\approx 35\ \mathrm{J\ m^{-2}}$. Invoking equation (5.1), the coercive stress is inferred to be $\tau^T=580$ MPa. This is, indeed, within the measured range (figure 3; Baither *et al.* 2001). It is pertinent to recall, however, that the τ^T measurements refer to stress-induced *domain wall motion* (Baither *et al.* 2001), while the present toughening involves both *domain nucleation and propagation*. A proposed stress/strain curve for nucleation-controlled ferroelastic toughening is depicted on figure 5*b*.

If, as indicated by this work, ferroelasticity is the primary toughening mechanism in metastable YSZ, then materials with greater tetragonality would exhibit even higher levels of toughness. The veracity of this implication has been substantiated

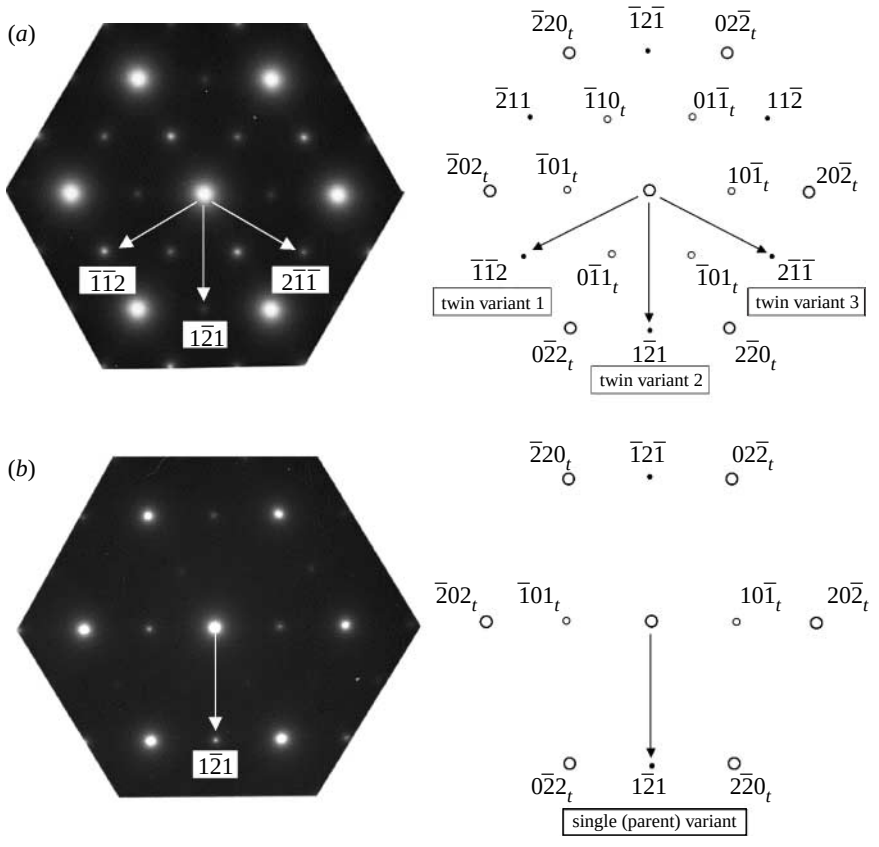

Figure 11. Selected area diffraction patterns of the ⟨111⟩ zone and corresponding schematics. (*a*) Grain within the process zone showing presence of all three twin variants. (*b*) A grain outside the process zone. Schematics of the patterns are included for ease of explanation.

by recent measurements conducted on a polycrystalline $(YO_{1.5}, TiO_2)ZrO_2$ ternary fabricated under similar conditions, having $c/a=1.023$, which exhibited unprecedented toughness for a t'-composition, $\Gamma_{ss}=89\ \mathrm{J\ m^{-2}}$ (Schaedler 2006). The caveat is that the coercive stress is also likely to change. For instance, lowering the magnitude of $\boldsymbol{\tau}^T$ increases the toughness because, in equation (5.1), the zone height scales is $h\sim 1/(\boldsymbol{\tau}^T)^2$ (Evans 1990). Moreover, it remains to be established that the same ferroelastic toughening mechanism occurs in the single crystal columns found in the coatings deposited using electron beam methods.

6. Conclusion

The toughness of 7 wt% YSZ with the metastable tetragonal-prime (t') structure has been investigated. A ferroelastic mechanism has been explored by characterizing the wake of an indentation-induced crack by using TEM and high-resolution optical interferometry. A crack process zone approximately 3 μm in width, containing a high density of nanoscale, twin-related, domains has been identified,

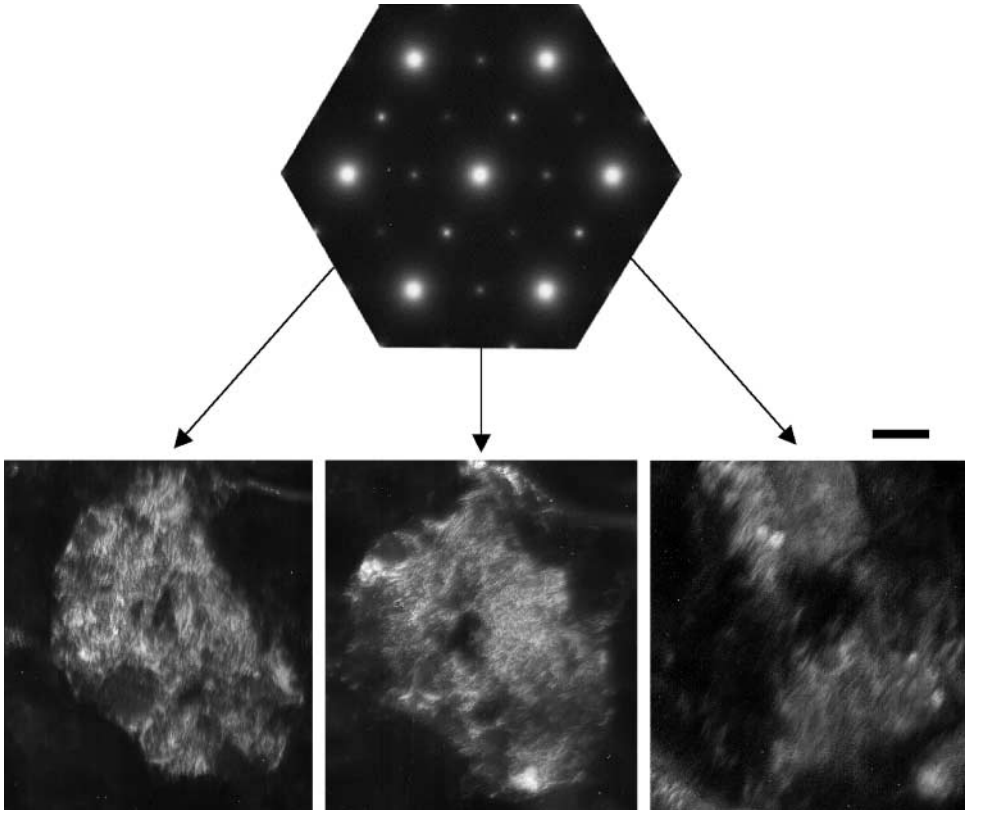

Figure 12. Dark-field imaging of the {112} reflections from a grain within the process zone, indicating approximately equal incidence of all three twin variants. Scale bar, 500 nm.

consistent with a ferroelastic mechanism. Dark-field imaging by TEM has revealed equal proportions of all-three twin variants within the process zone. Such domains are not present in the virgin material remote from the process zone. Consequently, the toughening mechanism appears to be controlled by the *nucleation of domains* rather than the motion of pre-existing domain boundaries. Based on the measured process zone size and the strains attributable to the tetragonality, it has been shown that the measured toughness is consistent with a ferroelastic mechanism for a reasonable coercive stress. One implication is that oxides with still greater tetragonality have the possibility of even higher toughness than the t'-7 wt% YSZ compositions used in current thermal barrier systems.

The authors are grateful to Prof. Manfred Rühle for discussions on interpreting electron microscopy observations of ferroelastic domains in zirconia. We also acknowledge research support from the Office of Naval Research (MURI/N00014-00-1-0438).

References

Anstis, G. R., Chantikul, P., Lawn, B. R. & Marshall, D. B. 1981 A critical evaluation of indentation techniques for measuring fracture toughness: I, direct crack measurements. *J. Am. Cer. Soc.* **64**, 533–538. (doi:10.1111/j.1151-2916.1981.tb10320.x)

Baither, D., Bartsch, M., Baufeld, B., Tikhonovsky, A., Foitzik, A., Rühle, M. & Messerschmidt, U. 2001 Ferroelastic and plastic deformation of t'-zirconia single crystals. *J. Am. Cer. Soc.* **84**, 1755–1762.

Becher, P. F. & Swain, M. V. 1992 Grain-size-dependent transformation behavior in polycrystalline tetragonal zirconia. *J. Am. Cer. Soc.* **75**, 493–502. (doi:10.1111/j.1151-2916.1992.tb07832.x)

Borom, M. P., Johnson, C. A. & Peluso, L. A. 1996 Role of environment deposits and operating surface temperature in spallation of air plasma sprayed thermal barrier coatings. *Surf. Coat. Technol.* **86-87**, 116–126. (doi:10.1016/S0257-8972(96)02994-5)

Chan, C-J., Lange, F. F., Rühle, M., Jue, J.-F. & Virkar, A. V. 1991 Ferroelastic domain switching in tetragonal zirconia single crystals—microstructural aspects. *J. Am. Cer. Soc.* **74**, 807–813. (doi:10.1111/j.1151-2916.1991.tb06929.x)

Chen, X., Wang, R., Yao, N., Evans, A. G., Hutchinson, J. W. & Bruce, R. W. 2003 Foreign object damage in a thermal barrier system: mechanisms and simulations. *Mater. Sci. Eng. A* **352**, 221–231. (doi:10.1016/S0921-5093(02)00905-x)

Choi, S. R., Hutchinson, J. W. & Evans, A. G. 1999 Delamination of multilayer thermal barrier coatings. *Mech. Mater.* **31**, 431–447. (doi:10.1016/S0167-6636(99)00016-2)

Clarke, D. R. & Adar, F. 1982 Measurement of the crystallographically transformed zone produced by fracture in ceramics containing tetragonal zirconia. *J. Am. Cer. Soc.* **65**, 284–288. (doi:10.1111/j.1151-2916.1982.tb10445.x)

Clarke, D. R. & Levi, C. G. 2003 Materials design for the next generation thermal barrier coatings. *Annu. Rev. Mater. Res.* **33**, 383–417. (doi:10.1146/annurev.matsci.33.011403.113718)

Cook, R. F. & Pharr, G. M. 1990 Direct observation and analysis of indentation cracking in glasses and ceramics. *J. Am. Cer. Soc.* **73**, 787–817. (doi:10.1111/j.1151-2916.1990.tb05119.x)

Evans, A. G. 1990 Perspective on the development of high-toughness ceramics. *J. Am. Cer. Soc.* **73**, 187–206. (doi:10.1111/j.1151-2916.1990.tb06493.x)

Evans, A. G. & Cannon, R. M. 1986 Overview no. 48: toughening of brittle solids by martensitic transformations. *Acta Metall.* **34**, 761–800. (doi:10.1016/0001-6160(86)90052-0)

Evans, A. G. & Charles, E. A. 1976 Fracture toughness determinations by indentation. *J. Am. Cer. Soc.* **59**, 371. (doi:10.1111/j.1151-2916.1976.tb10991.x)

Evans, A. G., Mumm, D. R., Hutchinson, J. W., Meier, G. H. & Pettit, F. S. 2001 Mechanisms controlling the durability of thermal barrier coatings. *Prog. Mater. Sci.* **46**, 505–553. (doi:10.1016/S0079-6425(00)00020-7)

Green, D. J., Hannink, R. H. J. & Swain, M. V. 1989 *Transformation toughening of ceramics*. Boca Raton, FL: CRC Press.

Jue, J.-F. & Virkar, A. V. 1990 Fabrication microstructural characterization, mechanical properties of polycrystalline t'-zirconia. *J. Am. Cer. Soc.* **73**, 3650–3657. (doi:10.1111/j.1151-2916.1990.tb04271.x)

Lange, F. F. 1982 Transformation toughening part 3: experimental observations in the ZrO_2–Y_2O_3 system. *J. Mater. Sci.* **17**, 240–246. (doi:10.1007/BF00809059)

Lawn, B. R. 1975 *Fracture of brittle solids*. Cambridge, UK: Cambridge University Press.

Levi, C. G. 2004 Emerging materials, processes for thermal barrier systems. *Curr. Opin. Solid State Mater. Sci.* **8**, 77–91. (doi:10.1016/j.cossms.2004.03.009)

Marrow, T. J., Roberts, S. G. & Pearce-Higgins, A. K. 1994 The brittle/ductile transition in cubic stabilised zirconia. *J. Eur. Cer. Soc.* **14**, 447–453. (doi:10.1016/0955-2219(94)90083-3)

Mercer, C., Faulhaber, S., Evans, A. G. & Darolia, R. 2005 Foreign object damage in a thermal barrier system: mechanisms and simulations. *Acta Mater.* **53**, 1029–1039. (doi:10.1016/j.actamat.2004.11.028)

Mumm, D. R., Evans, A. G. & Spitsberg, I. T. 2001 Characterization of a cyclic displacement instability for a thermally grown oxide in a thermal barrier system. *Acta Mater.* **49**, 2329–2340. (doi:10.1016/S1359-6454(01)00071-4)

Nychka, J. A., Winter, M. R., Clarke, D. R., Naganuma, T. & Kagawa, Y. 2006 Temperature-dependent optical reflectivity of tetragonal-prime yttria-stabilized zirconia. *J. Am. Cer. Soc.* **89**, 908–913. (doi:10.1111/j.1551-2916.2005.00813.x)

Schaedler, T. 2006, Phase evolution in the $YO_{1.5}$–TiO_2–ZrO_2 system and effects on ionic conductivity and toughness. Ph.D. dissertation, Materials Department, University of California Santa Barbara.

Schulz, U., Terry, S. G. & Levi, C. G. 2003 Microstructure and texture of EB-PVD TBCs grown under different rotation modes. *Mater. Sci. Eng. A* **360**, 319–329. (doi:10.1016/S0921-5093(03)00470-2)

Srinivasan, G. V., Jue, J.-F., Kuo, S.-Y. & Virkar, A. V. 1989 Ferroelastic domain switching in polydomain tetragonal zirconia single crystals. *J. Am. Cer. Soc.* **72**, 2098–2103. (doi:10.1111/j.1151-2916.1989.tb06038.x)

Suo, Z. & Hutchinson, J. W. 1989 Steady-state cracking in brittle substrates beneath adherent films. *Int. J. Solids Struct.* **25**, 1337–1353. (doi:10.1016/0020-7683(89)90096-6)

Tolpygo, V. K. & Clarke, D. R. 1999 Tensile cracking during thermal cycling of alumina films formed by high-temperature oxidation. *Acta Mater.* **47**, 3589–3605. (doi:10.1016/S1359-6454(99)00216-5)

Virkar, A. V. & Matsumoto, R. L. K. 1986 Ferroelastic domain switching as a toughening mechanism in tetragonal zirconia. *J. Am. Cer. Soc.* **69**, C-224–C-226. (doi:10.1111/j.1151-2916.1986.tb07341.x)

Wachtman, J. B. 1996 *Mechanical properties of ceramics*. New York, NY: Wiley.

Watanabe, M., Mercer, C., Levi, C. G. & Evans, A. G. 2004 A probe for the high temperature deformation of thermal barrier oxides. *Acta Mater.* **52**, 1479–1487. (doi:10.1016/j.actamat.2003.11.029)